Functional repair after ischemic injury through high efficiency *in situ* astrocyte-to-neuron conversion

Yuchen Chen[1], Ningxin Ma[1], Zifei Pei[1], Zheng Wu[1], Fabricio H. Do-Monte[2,4], Pengqian Huang[1], Emma Yellin[1], Miranda Chen[1], Jiuchao Yin[1], Grace Lee[1], Angélica Minier-Toribio [2], Yi Hu[1], Yuting Bai[1], Kathryn Lee[1], Gregory J. Quirk[2], Gong Chen[1,3]*

1. Department of Biology, Huck Institutes of Life Sciences, Pennsylvania State University, University Park, PA 16802, USA.
2. Departments of Psychiatry and Anatomy & Neurobiology, University of Puerto Rico School of Medicine, P.O. Box 365067, San Juan, Puerto Rico 00936-5067
3. Guangdong-Hongkong-Macau Institute of CNS Regeneration, Jinan University, Guangzhou 510632, China.
4. Present address: Department of Neurobiology and Anatomy, McGovern Medical School, The University of Texas Health Science Center, Houston, Texas 77030, USA.

Keywords: NeuroD1, ischemic injury, brain repair, astrocyte-to-neuron conversion, motor function, fear conditioning learning.

***Correspondence should be addressed to**:

Gong Chen, Ph.D.
Professor and Verne M. Willaman Chair in Life Sciences
Department of Biology, Huck Institutes of Life Sciences,
The Pennsylvania State University, University Park, PA 16802, USA.
Email: gongchen@psu.edu
Phone: 814-865-2488
Website: http://bio.psu.edu/directory/guc2

ABSTRACT

Mammalian brains have largely lost internal neural regeneration capability except for a few discrete neurogenic niches. After brain injury, the cerebral cortex is especially difficult to repair due to its extremely low rate of adult neurogenesis. Previous studies have converted glial cells into neurons, but the total number of neurons generated is rather limited, casting doubt about its therapeutic potential. Here, we demonstrate that high-efficiency neuroregeneration can be achieved in adult mammalian brains by making use of an engineered AAV Cre-FLEX system to convert a large number of reactive astrocytes into functional neurons. Specifically, using a combination of GFAP::Cre and FLEX-NeuroD1 AAV system, we were able to regenerate enough new neurons from astrocytes to cover about 40% of the neurons lost from an ischemic injury (400 NeuN+ new neurons/mm2), compared to previously reported an average of <1% of cortical neurons (2-8 NeuN+ neurons/mm2) in an ischemic-injured adult mammalian cortex. Importantly, this in situ astrocyte-to-neuron conversion process also improved survival of injured pre-existing neurons, (additional 400 neurons/mm2), leading to a repaired motor cortex with layered cortical structures. Moreover, NeuroD1-converted neurons not only form functional neural circuits but also rescue motor and memory deficits after ischemic injury. Our results establish the proof-of-principle that a highly efficient in situ astrocyte-to-neuron conversion approach provides a novel treatment for neurological disorders that are in need of new neurons.

53 **INTRODUCTION**

54

55 Neuronal loss is a major pathological hallmark of brain injury. Regenerating new
56 neurons to replenish lost neurons after an injury is critical for the brain repair.
57 Unfortunately, adult mammalian brains have largely lost active neurogenesis capacity,
58 except a few neurogenic niches such as hippocampus and subventricular zone (SVZ) [1].
59 For example, after ischemic injury, the number of new neurons generated through the
60 internal neurogenesis is reported to be less than 1% of total lost neurons in adult
61 mammalian brains [2-5]. Interestingly, even the neural stem cells (NSCs) originating from
62 the SVZ mostly produce reactive astrocytes, not neurons, after migrating to injured
63 cortical areas [6, 7]. As an alternative, engrafting external NSCs has been explored for
64 post-stroke treatment [8-10], but immunorejection, tumorigenesis, and long-term survival
65 are challenges to this approach [11, 12]. Therefore, it is urgent to develop new approaches
66 to regenerate a sufficient number of new neurons in order to achieve long-term
67 functional recovery after the brain injury.

68 We have recently demonstrated the direct conversion of reactive astrocytes into
69 functional neurons by a single transcription factor NeuroD1 in the mouse brain [13]. Other
70 groups also reported conversion of glial cells into neurons both *in vitro* and *in vivo* [13-21].
71 While the *in vivo* glia-to-neuron conversion approach can regenerate new neurons
72 inside mouse brain and spinal cord, it is unclear whether this emerging new technology
73 can generate sufficient numbers of new neurons for therapeutic applications. In the
74 present study, we report that by using an engineered AAV Cre-FLEX system to
75 ectopically express NeuroD1 in reactive astrocytes in a focal ischemic injury model, we
76 are able to regenerate 400 new neurons per mm^2 in the mouse motor cortex and rebuild
77 the layered cortical structures. Behavioral tests indicate that NeuroD1-treatment
78 significantly rescues both motor deficits and fear memory deficits after the ischemic
79 injury in rodents. Together, our studies demonstrate that NeuroD1-mediated *in situ* cell
80 conversion not only converts astrocytes into functional new neurons but also rebuilds
81 neural circuits and rescues behavioral deficits, establishing a novel approach for
82 functional brain repair following the neural injury.

83 **RESULTS:**

84

85 **High efficiency of neuroregeneration achieved by AAV Cre-FLEX-NeuroD1 system**

86 We have recently demonstrated that NeuroD1 acts as a master transcription factor to
87 directly convert glial cells into functional neurons inside mouse brains [13]. However, the
88 total number of neurons generated is rather limited, raising concerns whether this novel
89 *in situ* cell conversion technology has real clinical value[22]. In this study, we used focal
90 ischemic injury as a model system to investigate whether the *in situ* cell conversion
91 approach can achieve functional brain repair. We elicited focal ischemic injury by
92 injecting vasoconstrictive peptide endothelin-1 (ET-1, 1-31) into the motor cortex of FVB
93 mice, producing a significant tissue damage progressively up to 10 weeks following the
94 ischemic injury (Fig. 1a,b) [23-26]. To convert reactive astrocytes into neurons, we
95 surveyed the injury areas at different time points after ischemic insult and found that
96 astrocytes were not reactive at five days post stroke (dps) (Fig. 1c) but then started to
97 show a significant accumulation of GFAP, a commonly used reactive astrocyte marker,
98 at 10 dps (Fig. 1d). Consistent with our previous report [13], injection of retroviruses
99 expressing NeuroD1 at 10 dps resulted in successful conversion of reactive glial cells
100 into NeuN-positive neurons (Fig. 1e). However, the number of neurons was limited due
101 to the fact that retroviruses were only able to express NeuroD1 in the dividing reactive
102 glial cells. To increase the number of neurons, we used adeno-associated virus (AAV)
103 to infect both dividing and non-dividing glial cells. AAV has advantages such as high
104 infection rate and low pathogenicity in humans, and importantly, has been approved by
105 FDA for clinical trials in the treatment of CNS disorders [27]. To infect astrocytes
106 specifically, we firstly constructed an AAV vector (recombinant serotype AAV9)
107 expressing NeuroD1 under the direct control of a human GFAP promoter
108 (hGFAP::NeuroD1-P2A-GFP). As expected, AAV NeuroD1 successfully converted
109 astrocytes into NeuN-positive neurons (Fig. 1f). While the number of neurons increased
110 significantly using AAV hGFAP::NeuroD1-GFP in comparison with that of retroviruses,
111 the hGFAP promoter can be down-regulated during the astrocyte-to-neuron (AtN)
112 conversion, making this process less complete and less efficient. The reduction of GFP
113 expression under the direct control of GFAP promoter also makes it difficult to

114 distinguish the converted from non-converted neurons. In order to target astrocytes
115 specifically for cell conversion while keeping a high expression level of NeuroD1, we
116 decided to separate the GFAP promoter and NeuroD1 into two different AAV vectors by
117 using the Cre-FLEX (flip-excision) homologous recombination system [28]. One vector
118 contains a human GFAP promoter to drive the expression of Cre recombinase
119 (hGFAP::Cre) in astrocytes. The second vector contains two pairs of heterotypic,
120 antiparallel loxP-type recombination sites flanking an inverted sequence of NeuroD1-
121 P2A-GFP (or NeuroD1-P2A-mCherry) under the control of a constitutive promoter CAG
122 (CAG::FLEX-NeuroD1-P2A-GFP/mCherry) (Supplementary Fig. 1). The advantage of
123 this AAV Cre-FLEX system is that the Cre expression is controlled by the hGFAP
124 promoter to maintain the specificity towards astrocytes, while NeuroD1 expression is
125 driven by the CAG promoter to avoid being silenced during AtN conversion. Indeed, with
126 this Cre-FLEX system, a strong expression of NeuroD1 in reactive astrocytes was
127 confirmed by immunostaining as early as 4 days post-viral injection (4 dpi) (Fig. 1g, top
128 row). Interestingly, some NeuroD1 AAV-infected astrocytes were clearly captured in a
129 transitional stage toward neurons, showing co-immunostaining of both NeuN and GFAP
130 (Fig. 1g, bottom row). Remarkably, using our AAV Cre-FLEX system, we detected a
131 large number of NeuroD1-converted neurons in the injured mouse cortex (Fig. 1h, i),
132 which was not possible using the other viruses we had tried.
133

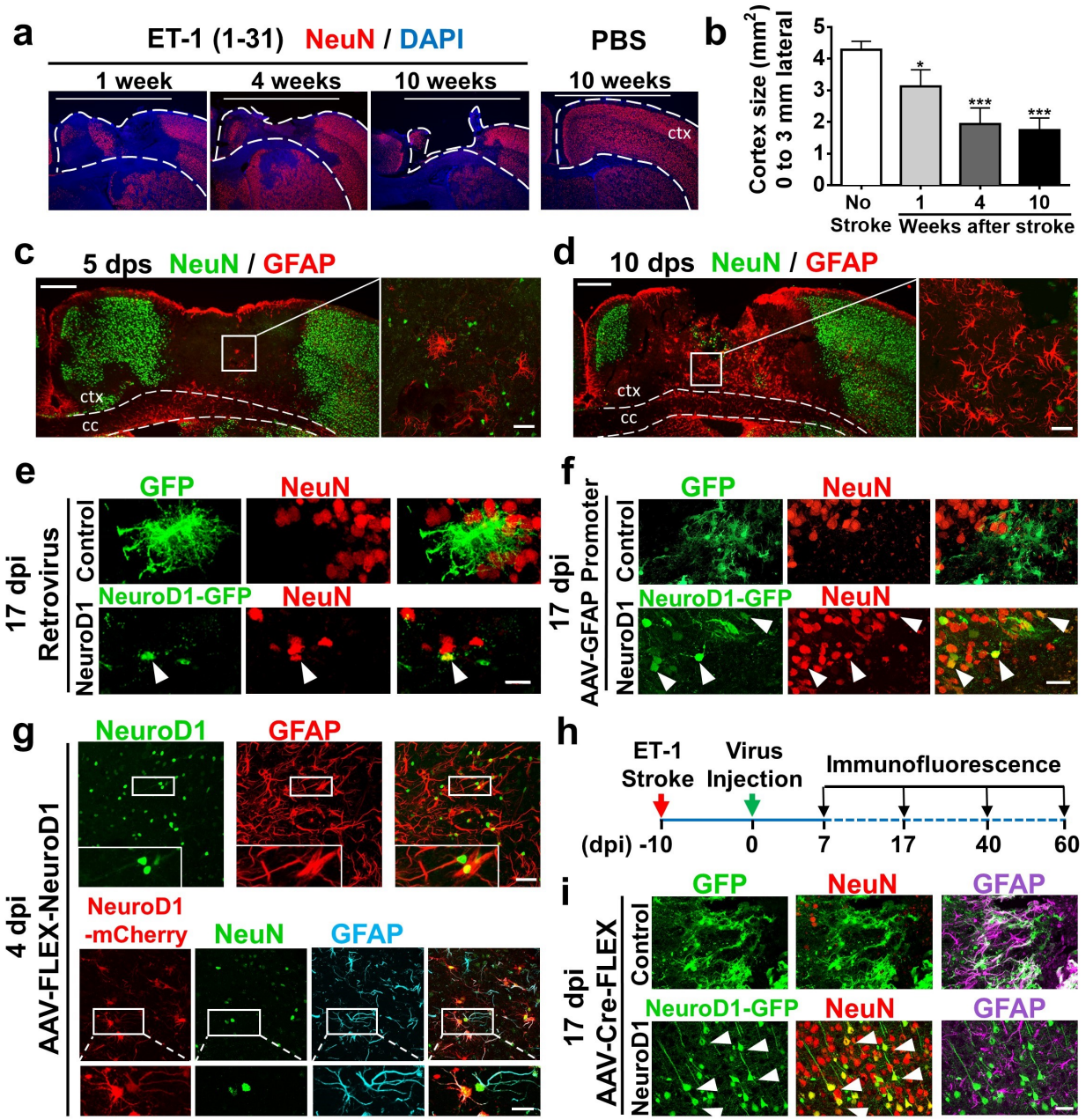

Figure 1. NeuroD1-mediated astrocyte-to-neuron conversion in a focal ischemic injury model. **(a)** Tissue loss caused by focal ischemic injury. Injection of endothelin-1 (ET-1, 1-31) into mouse motor cortex led to a gradual tissue loss in 10 weeks. Dashed lines indicate cortical areas. **(b)** Quantification of the remaining cortical tissue (from the midline to 3 mm lateral area, white bar) at 1, 4 and 10 weeks after ischemic injury in the motor cortex (n = 3 for each time point). **(c, d)** Assessing reactive astrocytes after ischemic injury. Immunostaining of NeuN and GFAP at 5 days (**c**) and 10 days post

142 stroke (dps) (**d**) revealed reactive astrocytes at 10 dps. c.c., corpus callosum. ctx,
143 cortex. **(e)** Retroviruses expressing GFP alone (top row) or NeuroD1-GFP (bottom row),
144 illustrating neuronal conversion by NeuroD1. Viral injection at 10 dps and
145 immunostaining at 17 days post viral injection (dpi). **(f)** Injection of AAV9 expressing
146 GFP alone (hGFAP::GFP, top row) or NeuroD1-GFP (hGFAP::NeuroD1-P2A-GFP,
147 bottom row), illustrating more neurons generated by AAV than retroviruses. **(g)** Capture
148 of the transitional stage from astrocytes (GFAP) to neurons (NeuN) at early time points
149 of NeuroD1 expression (4 dpi). Injection of AAV9 hGFAP::Cre and CAG::FLEX-
150 NeuroD1-P2A-mCherry resulted in significant NeuroD1 expression in GFAP-labeled
151 astrocytes (top row). Interestingly, some NeuroD1-mCherry labeled cells showed both
152 NeuN and GFAP signal (bottom row), suggesting a transition stage from astrocytes to
153 neurons. **(h)** Experimental outline for ischemic injury, AAV injection (Cre-FLEX system),
154 and immunostaining analysis. **(i)** Detection of a large number of NeuroD1-converted
155 neurons using AAV Cre-FLEX system. At 17 dpi, the GFP control group showed many
156 GFAP+ reactive astrocytes (top row, GFAP in purple), whereas the majority of
157 NeuroD1-GFP labeled cells became NeuN-positive (red) neurons (bottom row). Scale
158 bar: **(a)** 3 mm; **(c, d)** Left panel 200 μm, Right panel 40 μm. **(e)** 20 μm. **(f, i)** 40 μm; **(g)**
159 40 μm (inset 20 μm).

160

161 **Neural repair after astrocyte-to-neuron conversion**

162 After achieving high efficiency of neuroregeneration using AAV Cre-FLEX system, we
163 investigated the total number of neurons in NeuroD1-infected areas (Fig. 2a).
164 Compared to the cortex infected with control viruses, NeuroD1 AAV-infected cortex
165 showed many more NeuN+ neurons (red) and less tissue damages (Fig. 2a, left panels
166 in low power). Interestingly, in the NeuroD1 AAV-infected areas, GFAP-labeled
167 astrocytes (purple) persisted and intermingled with NeuroD1-converted neurons,
168 indicating that astrocytes were not depleted by AtN conversion (Fig. 2a, right panels in
169 high power). Surprisingly, after NeuroD1-mediated AtN conversion, we not only
170 detected NeuroD1 positive neurons (green and yellow) but also many non-converted
171 neurons (Fig. 2b, NeuroD1-, red only). Quantitative analysis revealed that ~40% of
172 NeuN+ neurons in the injury areas were NeuroD1-positive and ~60% of neurons were

173 NeuroD1-negative (Fig. 2c; Control group: NeuN+, 27.1 ± 8.1 / 0.1 mm^2; NeuroD1
174 group: NeuroD1-/NeuN+, 64.9 ± 7.9 / 0.1 mm^2; NeuroD1+/NeuN+, 39.9 ± 2.4 / 0.1 mm^2;
175 n = 3 mice per group). Notably, the non-converted neurons in the NeuroD1-treated
176 areas also more than doubled the total number of neurons in the control GFP-infected
177 areas (Fig. 2c), suggesting that NeuroD1-mediated AtN conversion significantly
178 enhances the survival of pre-existing neurons. Overall, there were more than three
179 times as many NeuN+ neurons in the NeuroD1-infected areas than the controls.
180 Therefore, efficient *in situ* AtN conversion not only regenerated new neurons but also
181 protected injured neurons from further damage from the surrounding toxic environment.
182 In accordance with a significant increase in the total number of neurons after
183 NeuroD1-treatment, immunostaining of neuronal dendritic markers MAP2 and SMI32
184 showed clearly aligned dendrites in the NeuroD1 group, compared to the rather
185 disorganized pattern in GFP controls (Fig. 2d,e). Similarly, using axonal marker SMI312
186 and NF200 along with myelination marker MBP, we found more axons in the NeuroD1
187 group (Fig. 2f), and these were also highly myelinated (Fig. 2g). Signal intensity and
188 coverage area for these markers are shown in Supplementary Fig. 2. To corroborate
189 with the immunostaining results, we further performed RT-PCR experiments and found
190 that the expression of neuronal genes including *NeuN*, *Robo2*, and *Syn1* all showed a
191 remarkable decrease after the ischemic injury, but significantly rescued by NeuroD1-
192 treatment (Fig. 2h). Moreover, we quantified the total number of NeuN+ neurons within
193 the ischemic areas at different time points following AAV infection. After ischemic injury,
194 the total number of NeuN-positive neurons in the control group was only ~20% of the
195 non-injured brains, indicating that 80% of neurons were lost or injured in our severe
196 focal ischemic injury model. However, in the NeuroD1 group, the NeuN+ neurons
197 showed a significant recovery over the 60 days following viral injection and reached
198 ~70% of the non-injury level (Fig. 2i). Such a significant increase in the total number of
199 cortical neurons after NeuroD1-treatment provides sufficient number of neurons for
200 further functional recovery.
201

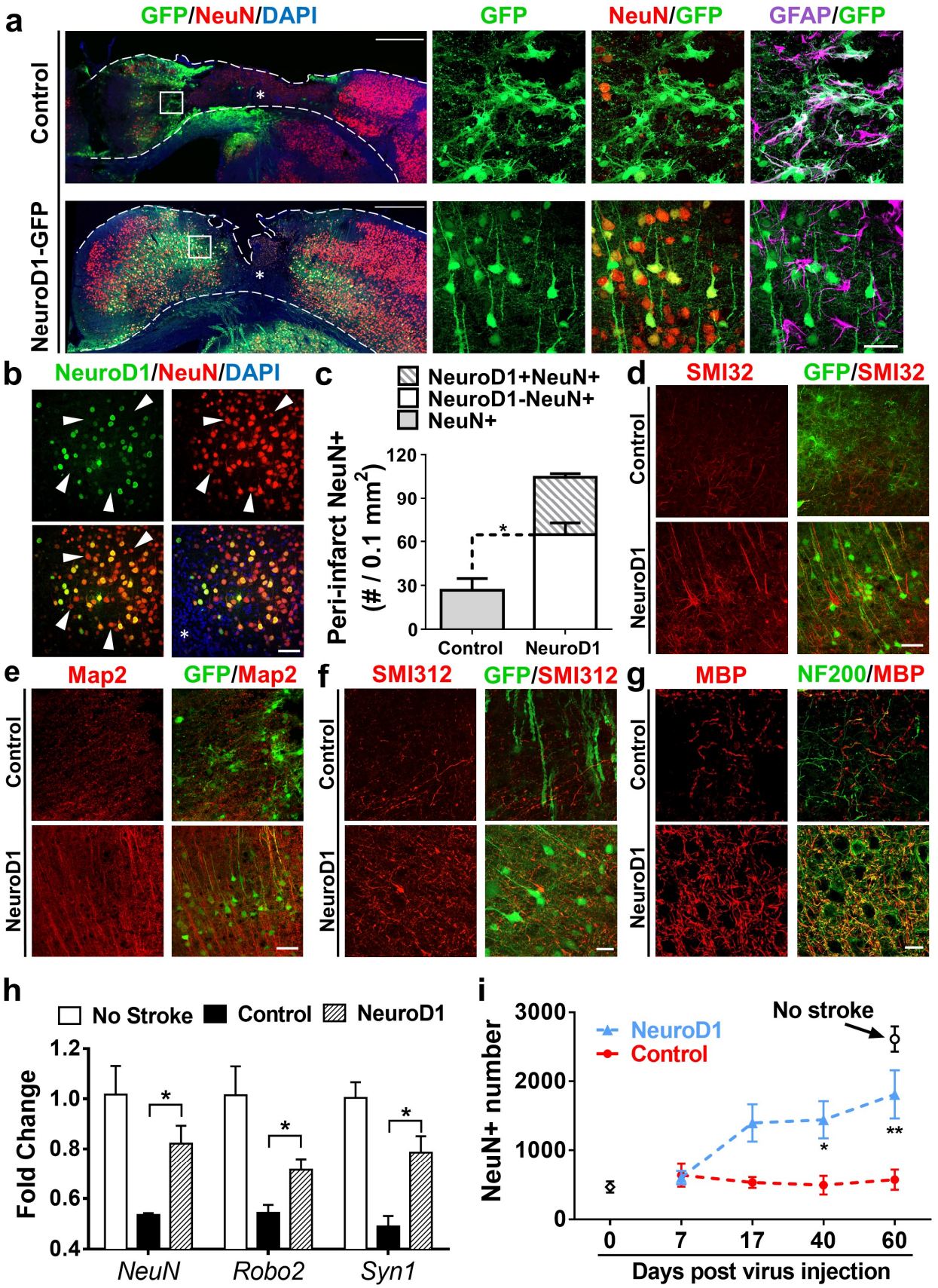
a
GFP/NeuN/DAPI
GFP
NeuN/GFP
GFAP/GFP
Control
NeuroD1-GFP
b
NeuroD1/NeuN/DAPI
c
NeuroD1+NeuN+
NeuroD1-NeuN+
NeuN+
Peri-infarct NeuN+ (# / 0.1 mm2)
120
90
60
30
0
Control
NeuroD1
d
SMI32
GFP/SMI32
Control
NeuroD1
e
Map2
GFP/Map2
Control
NeuroD1
f
SMI312
GFP/SMI312
Control
NeuroD1
g
MBP
NF200/MBP
Control
NeuroD1
h
No Stroke
Control
NeuroD1
Fold Change
1.2
1.0
0.8
0.6
0.4
NeuN
Robo2
Syn1
i
No stroke
NeuroD1
Control
NeuN+ number
3000
2000
1000
0
0
7
17
40
60
Days post virus injection

202

203 **Figure 2.** High efficiency of neuroregeneration achieved by NeuroD1-mediated
204 astrocyte-to-neuron conversion in the ischemic injury areas. **(a)** Comparison of the
205 motor cortex (17 dpi) between the control (top row) and NeuroD1 group (bottom row).
206 Left panels showing the overall cortical morphology after ischemic injury and viral
207 treatment, while right panels showing enlarged images of the peri-infarct areas. Note
208 that NeuroD1-infected cells (green) were mostly converted into NeuN+ neurons
209 (yellow), but GFAP+ astrocytes (purple) still persisted in the same areas. **(b)** NeuroD1-
210 converted neurons (green and yellow) were intermingled with non-converted neurons
211 (red, arrowheads) in the injury areas. **(c)** Quantification of total NeuN+ cells in the peri-
212 infarct areas of control group and NeuroD1 group. Note that the number of non-
213 converted neurons in the NeuroD1 group (white bar) more than doubled the number in
214 the control group, suggesting a neuroprotective effect of NeuroD1 conversion. n = 3
215 mice in each group. * P < 0.05. **(d, e)** Immunostaining of neuronal dendrite markers
216 SMI32 **(d)** and MAP2 **(e)** showing much improved neuronal morphology in the NeuroD1
217 group (bottom row) compared to the control group (top row). **(f, g)** Immunostaining of
218 axonal marker SMI312 **(f)**, NF200 **(g)** and axon myelination marker MBP **(g)** showed
219 increased axons and axonal myelination in the NeuroD1 group (bottom row) compared
220 to the control group (top row). **(h)** RT-PCR analysis revealed a significant increase of
221 neuronal mRNA level including NeuN, Robo2 and Syn1 after NeuroD1 treatment. * P <
222 0.05. n = 4 mice each group. **(i)** Quantification of the total number of NeuN+ cells in the
223 motor cortical areas (500-2500 μm lateral from the midline). Note a significant increase
224 of the total number of neurons in the NeuroD1 group by 60 dpi. n = 3 mice in each
225 group. * P < 0.05, ** P < 0.01, Two-way ANOVA followed by Sidak's multiple
226 comparison tests. Data are represented as mean ± s.e.m. Scale bar: **(a)** 500 μm for left
227 panels; 40 μm for right panels; **(b, d, e)** 40 μm; **(f, g)** 20 μm.

228

229

230 **Reconstitution of motor cortex after neuronal conversion**

231 One pivotal question regarding *in situ* AtN conversion is whether the newly converted
232 neurons can form functional neural circuits. To answer this question, we first examined
233 the cortical structures after ischemic injury with or without NeuroD1-mediated AtN

234 conversion. Over the time course of two months, we observed a gradual cortical tissue
235 loss in the control group injected with the control virus (Fig. 3a, top row), indicating the
236 severe brain injury. In contrast, the cortical tissue was largely preserved in the
237 NeuroD1-treated group without significant atrophy in the motor cortex area (Fig. 3a,
238 bottom row). Notably, after 60 days of NeuroD1 infection, we observed clearly layered
239 structures in the motor cortex of NeuroD1-treated animals (Fig. 3a and 3c, 60 dpi,
240 NeuroD1 images), suggesting reconstitution of cortical circuits after NeuroD1-treatment.
241 Quantitative analysis of the motor cortex revealed that the control group lost 70% of the
242 injured tissue over a 2-month period, whereas the NeuroD1-treated group only lost 20%
243 (Fig. 3b). Besides tissue preservation, we further discovered that the NeuroD1-
244 converted neurons sent their projections globally to many brain regions, including
245 ipsilateral and contralateral areas. For example, a sagittal section of the mouse brain
246 revealed that the NeuroD1-converted neurons projected axons from the motor cortex to
247 the ipsilateral striatum, thalamus, and hypothalamus (Fig. 3c). Coronal section of the
248 motor cortex showed that NeuroD1-converted neurons projected their axons to the
249 contralateral cortical regions through the corpus callosum (Supplementary Fig. S3).
250 Thus, NeuroD1-converted neurons can integrate into global brain circuits.
251
252
253 **Synaptic connection after neuronal conversion**

254 After morphological analysis of the structural recovery after *in situ* AtN conversion, we
255 further investigated functional recovery after NeuroD1-mediated AtN conversion.
256 Cortical slice recordings were performed on NeuroD1-converted neurons at 2 months
257 after viral injection (Fig. 3e, top images). Injecting depolarizing currents into the
258 NeuroD1-GFP labeled neurons triggered repetitive action potentials in every recorded
259 GFP+ neuron (n = 22) (Fig. 3e, bottom trace). To confirm that the recorded GFP+
260 neurons were converted by NeuroD1 rather than pre-existing neurons, we included
261 biocytin in our recording pipettes and performed immunostaining post whole-cell
262 recordings (Fig. 3f). As expected, the GFP+ neurons we recorded (labeled by biocytin,
263 red) were indeed NeuroD1-positive (cyan). Note that the biocytin immunostaining also
264 illuminated the complex dendrites of the NeuroD1-converted neurons after 2 months of

265 conversion (Fig. 3f), supporting their structural integration into the motor cortex after *in*
266 *situ* AtN conversion. Functionally, we detected robust spontaneous synaptic events,
267 both excitatory and inhibitory, in NeuroD1-converted neurons in the injury sites after 2
268 months of AtN conversion (Fig. 3g), suggesting that these neurons have functionally
269 integrated into the brain circuits through synaptic connections with other neurons.
270 Quantitative comparison between the GFP control and NeuroD1-GFP groups
271 demonstrated that the frequency of both EPSCs and IPSCs in the NeuroD1 group was
272 significantly higher than the control group (Fig. 3h; n = 22). Together, these data
273 demonstrate that NeuroD1-mediated AtN conversion can reconstitute functional neural
274 circuits after brain injury.

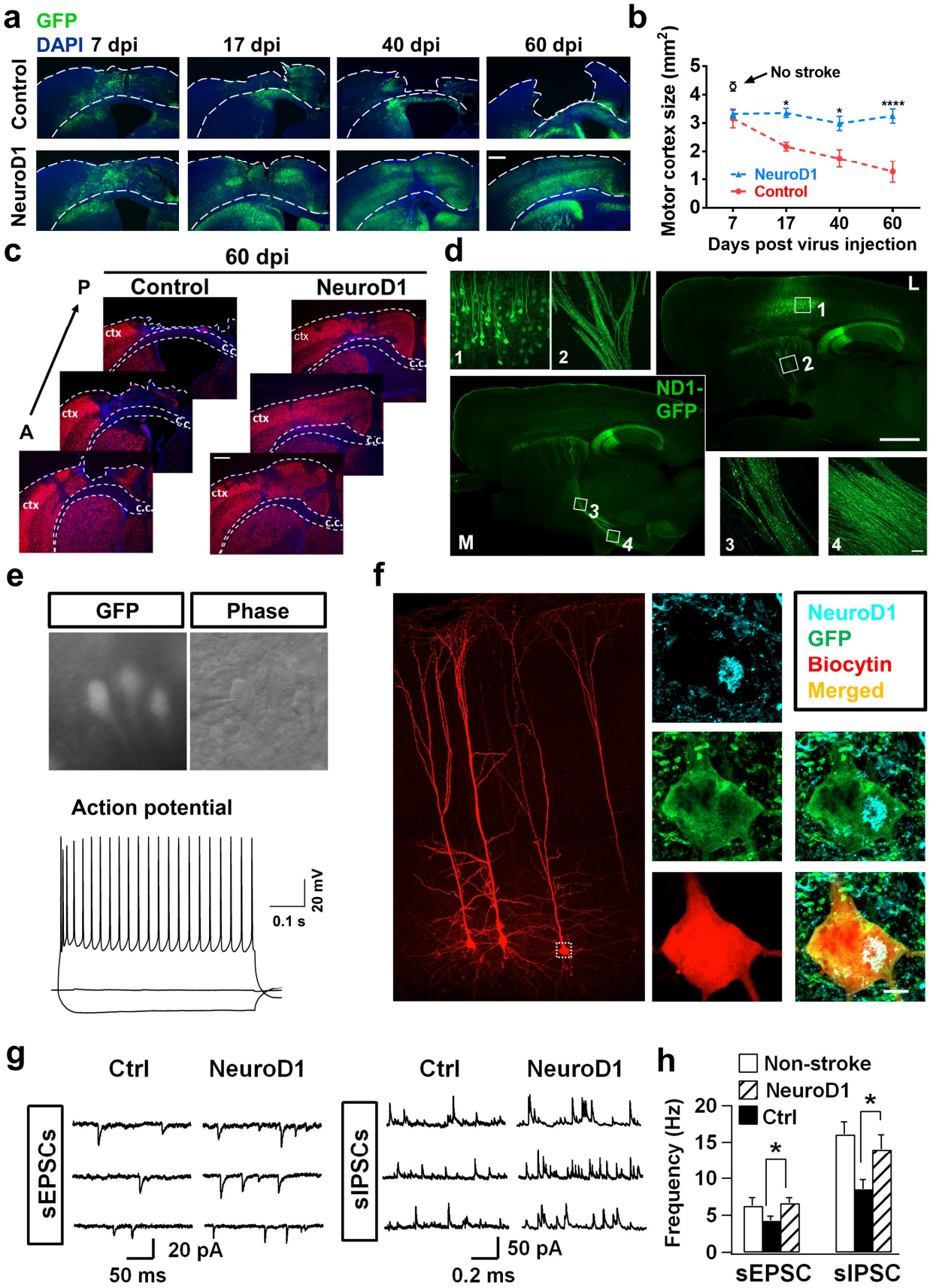
a
GFP
DAPI
7 dpi
17 dpi
40 dpi
60 dpi
Control
NeuroD1
b
Motor cortex size (mm²)
No stroke
NeuroD1
Control
Days post virus injection
c
60 dpi
Control
NeuroD1
P
A
ctx
d
L
M
ND1-GFP
e
GFP
Phase
Action potential
20 mV
0.1 s
f
NeuroD1
GFP
Biocytin
Merged
g
Ctrl
NeuroD1
sEPSCs
sIPSCs
20 pA
50 ms
50 pA
0.2 ms
h
Non-stroke
NeuroD1
Ctrl
Frequency (Hz)
sEPSC
sIPSC

275

276 **Figure 3.** Reconstitution of motor cortex with layered structures after NeuroD1-
277 treatment. **(a)** Low magnification images illustrating gradual tissue loss in the GFP
278 control group (top row), and the rescue by NeuroD1 treatment (bottom row). Note
279 layered structures in NeuroD1 group at 60 dpi. Dashed lines delineate the cortical
280 areas. **(b)** Quantification of the motor cortical areas (from midline to 3 mm lateral) in the
281 control versus NeuroD1 group. * $P < 0.05$, *** $P < 0.001$, Two-way ANOVA followed by
282 Sidak's multiple comparison test. n = 3 mice per group. **(c)** Serial brain sections from
283 anterior (A) to posterior (P) further illustrating severe tissue damage in the control
284 group. ctx, cortex; c.c., corpus callosum. **(d)** Representative images illustrating global
285 axonal projections from NeuroD1-converted neurons. Serial sagittal sections (17 dpi),
286 from medial (M, lower left) to lateral (L, upper right), showing converted neurons in the
287 cortex (inset 1), axonal bundles in the striatum (inset 2), thalamus (inset 3), and
288 hypothalamus (inset 4). **(e)** Brain slice recording on NeuroD1-converted neurons (GFP)
289 detected repetitive action potential firing (60 dpi, n = 22). **(f)** Biocytin (red) infusion in the
290 recording pipette during whole-cell recording followed with post-fix immunostaining
291 illustrating that the recorded neurons were indeed NeuroD1+ (cyan, 60 dpi). **(g)**
292 Representative traces of spontaneous excitatory (sEPSCs) and inhibitory synaptic
293 events (sIPSCs) recorded in NeuroD1-GFP labeled neurons (60 dpi). **(h)** Quantification
294 of the frequency of both sEPSCs and sIPSCs in cortical slices without injury (white bar),
295 or with ischemic injury (black bar, GFP control; striped bar, NeuroD1 group). Note that
296 NeuroD1 group showed significantly higher frequency of both sEPSCs and sIPSCs than
297 the control group (EPSC: control, 4.3 ± 0.6 Hz, n = 22; NeuroD1, 6.7 ± 0.8 Hz, n = 25; p
298 = 0.023, Student's *t* test) (IPSC: control, 8.6 ± 1.3 Hz, n = 22; NeuroD1, 14.0 ± 2.0 Hz, n
299 = 25; p = 0.032, Student's *t* test). Scale bars: **(a, c)** 400 μm; **(d)** 1000 μm for sagittal
300 images; 40 μm for inset images; **(f)** 200 μm for the left low magnification image; 5 μm
301 for right enlarged images.
302
303
304 **Functional rescue of motor deficits**
305 With a significant level of neuroregeneration in the injury areas after NeuroD1-mediated
306 AtN conversion, we then investigated whether NeuroD1 treatment can rescue motor

307 deficits caused by ischemic injury in the mouse motor cortex. We analyzed mouse
308 forelimb functions using three behavioral tests—food pellet retrieval, grid walking, and
309 cylinder test—at different time points following viral injection (Fig. 4a). To test for food
310 pellet retrieval, mice were deprived of food before the training and test to increase their
311 motivation for the food pellet. Before ischemic injury, normal animals could be trained to
312 retrieve 5-6 pellets on average out of total 8 pellets in 5 minutes. After ischemic injury,
313 their pellet retrieval capability was severely impaired, dropping to ~1 pellet on average
314 in 5 min (Fig. 4b). Then, the ischemic injured animals with similar motor deficits were
315 assigned into two groups for viral injection: one group injected with GFP viruses alone,
316 and the other injected with NeuroD1-GFP viruses. At 10 days after viral injection, there
317 was no significant difference between the two groups; but after 20 days of viral injection,
318 the NeuroD1 group started to show improvement in food pellet retrieval (Fig. 4b). By 60
319 days after viral injection, the NeuroD1 group reached ~4 pellets/5 min, whereas the
320 GFP control group could only retrieve <2 pellets/5 min (Fig. 4b). Similarly, for the grid
321 walking test, normal animals before injury had a low rate of foot fault, typically ~5% of
322 total steps within 5 minutes, while walking freely on a grid, but the foot fault rate
323 increased to over 10% after ischemic injury (Fig. 4c). After viral injection, the NeuroD1
324 group showed consistent improvement after 20 - 60 days of treatment, with the foot fault
325 rate decreasing to ~7%, whereas the GFP control group remained at a high foot fault
326 rate >9% (Fig. 4c). We also performed a cylinder test to assess the forelimb function
327 when animals rise and touch the sidewall of a cylinder. Normal animals typically use
328 both forelimbs to touch and push steadily against the sidewall, with a normal touching
329 rate ~85% (using both forelimbs). After a unilateral ischemic injury in the forelimb motor
330 cortex, the function of the impaired forelimb was significantly weakened and the
331 impaired limb often either failed to touch the sidewall or dragged along the wall after
332 briefly touching (Fig. 4d, normal touching rate dropped to ~35%). After 20 - 60 days of
333 viral infection, the NeuroD1 group showed a significant recovery in touching the sidewall
334 with the injured forelimb (~60%), whereas the majority of the GFP control mice still had
335 a weak forelimb affected by the ischemic injury (Fig. 4d). For all three tests, injection of
336 PBS as a sham control did not result in any behavioral deficits (black line in Fig. 4b-d),
337 and injection of ET-1 (1-31) without viral injection produced similar deficits as the GFP

control viral injection (orange line in Fig. 4b-d). Therefore, by using three different motor behavioral tests, we demonstrate that NeuroD1-treatment can rescue motor functional deficits following ischemic injury in the mouse motor cortex.

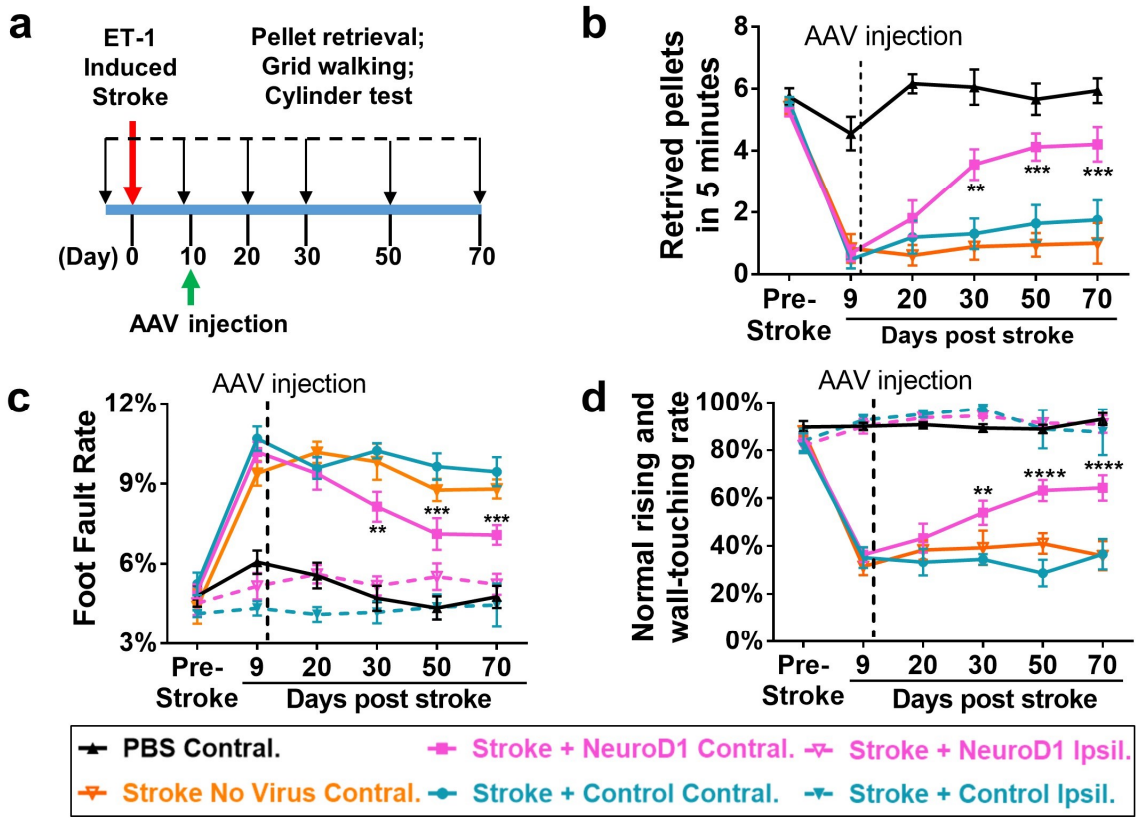

Figure 4. Motor functional improvement after NeuroD1-treatment. **(a)** Experimental design for mouse forelimb motor functional tests. Behavioral tests were conducted before ischemic injury to obtain baseline control, and then 9 dps but one day before viral injection to assess injury-induced functional deficits. AAV were injected at 10 dps, and behavioral tests were further performed at 20, 30, 50, and 70 dps to assess functional recovery. **(b)** Pellet retrieval test. NeuroD1 group (magenta) showed accelerated functional recovery compared to the control group (blue). Ischemic injury at the motor cortex severely impaired the food pellet retrieval capability, dropping from 5-6 pellets/5 min pre-stroke down to 1 pellet/5 min at 9 dps. After NeuroD1 treatment, pellet retrieval ability recovered to 4 pellets/5 min by 60 days post infection. Note that for food pellet retrieval test, only the motor cortex contralateral to the dominant side of forelimb was

354 injured and tested. ** P < 0.01, *** P < 0.001. Two-way ANOVA followed by Tukey
355 multiple comparison test. Data are represented as mean ± s.e.m. n = 12 mice for ET-1
356 plus control AAV group; n = 11 mice for ET-1 plus NeuroD1 AAV group; n = 6 mice for
357 ET-1 plus no virus group; and n = 6 mice for PBS control group. **(c)** Grid walking test.
358 NeuroD1 group showed lower foot fault rate compared to the control group. Ischemic
359 injury of the motor cortex significantly increased the foot fault rate, which was partially
360 rescued by NeuroD1 treatment. ** P < 0.01, *** P < 0.001. Two-way ANOVA followed by
361 Tukey multiple comparison test. Data are represented as mean ± s.e.m. n = 9 mice for
362 ET-1 plus control AAV contralateral group; n = 11 mice for ET-1 plus NeuroD1 AAV
363 contralateral group; n = 5 mice for ET-1 plus NeuroD1 ipsilateral group; and n = 5 mice
364 for ET-1 plus control ipsilateral group; n = 6 mice for ET-1 plus no virus contralateral
365 group; and n = 6 mice for PBS contralateral group. **(d)** Cylinder test. NeuroD1-treated
366 mice showed considerable recovery of rising and touching the sidewall with both
367 forelimbs compared to the control group. ** P < 0.01, **** P < 0.0001. Two-way ANOVA
368 followed by Tukey multiple comparison test. Data are represented as mean ± s.e.m. n =
369 9 mice for ET-1 plus control AAV contralateral group; n = 11 mice for ET-1 plus
370 NeuroD1 AAV contralateral group; n = 9 mice for ET-1 plus NeuroD1 ipsilateral group;
371 n = 7 mice for ET-1 plus control ipsilateral group; n = 6 mice for ET-1 plus no virus
372 contralateral group, n = 5 mice for PBS contralateral group.

373

374

375 **Functional rescue of memory deficits**

376 We next used a different animal species (rats instead of mice) and a different behavioral
377 task (cognitive rather than motor) to further test the effect of NeuroD1-mediated AtN
378 conversion following ischemic injury in the amygdala (Fig. 5). It is well established that
379 the associative memory of a conditioned stimulus (tone) and an aversive event
380 (electrical foot shock) is stored in the basolateral nucleus of the amygdala (BLA) [29, 30].
381 Lesions of the BLA impair both the acquisition and the subsequent retrieval of an
382 auditory fear memory [31, 32]. To assess the NeuroD1 effect on cognitive functions, rats
383 were injected with ET-1 into the BLA to produce an ischemic injury and then submitted
384 to auditory fear conditioning three weeks later (Fig. 5a). This interval was based on pilot

385 studies showing a significant impairment in fear acquisition combined with significant
386 neuronal injury approximately 21 days after the ET-1 stroke. The 21-day time point also
387 helped to maximize glial scar formation following ET-1 lesion (Abeysinghe et al., 2014),
388 an important factor to consider when using cell conversion strategies. ET-1 has been
389 previously used to induce ischemic lesions in rat models of stroke [23, 33]. Accordingly, we
390 found that intra-BLA infusion of ET-1 (1-21) (3 μl/side, 400 pmol) induced a robust
391 lesion in BLA (Supplementary Fig. S4). Behaviorally, rats infused with ET-1 showed a
392 significant reduction in the acquisition of a conditioned freezing response to the tone, in
393 comparison to a saline-infused control group (Fig. 5b, day 21). Reduced freezing was
394 also observed during the retrieval test the following day (Fig. 5b, day 22), suggesting
395 that the lesion induced by ET-1 impaired the formation of an auditory fear memory. One
396 day later, lesioned rats were separated into two groups receiving infusions of either
397 control virus or NeuroD1 virus (3 μl) into the BLA. After three weeks of viral infection,
398 animals were returned to the same box for a fear retrieval test (Fig. 5b, day 45). Rats in
399 the control group continued to show reduced freezing levels, as expected. In contrast,
400 freezing in the NeuroD1 group returned to the levels of the saline/saline group, and was
401 significantly higher than the group receiving the control virus infusion (Fig. 5b, day 45),
402 suggesting a rescue of the memory deficit by NeuroD1 treatment. There was no effect
403 of NeuroD1 on freezing during the pre-tone period (pre-CS, “x” symbol in Fig. 5b),
404 suggesting that NeuroD1 did not induce a general increase in amygdala excitability or
405 non-specific fear. After completion of behavioral tests, we performed immunostaining to
406 confirm viral infection in the BLA. As expected, we found that the majority of NeuroD1-
407 GFP-infected cells were NeuN-positive neurons (Fig. 5c). Together, these results
408 suggest that NeuroD1-treatment can rescue the fear memory deficits induced by an
409 ischemic lesion of BLA.
410

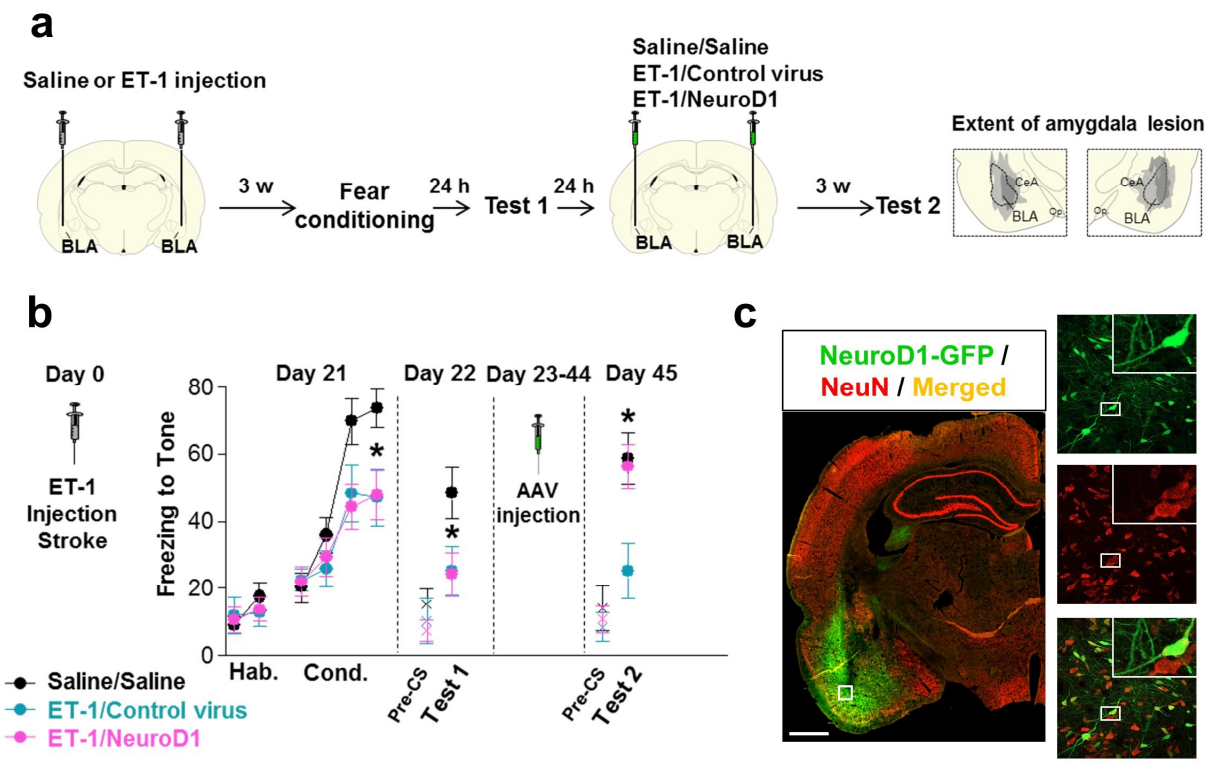

Figure 5. Recovery of fear conditioning memory after NeuroD1 treatment. **(a)** Experimental design of fear conditioning test in rats. ET-1 or saline was injected into the basolateral amygdala (BLA), followed by fear conditioning 3 weeks later. Fear memory tests were performed before viral injection and 3 weeks after viral injection to assess the retention of fear memory. Right two panels illustrate the amygdala lesion induced by the infusion of ET-1. Gray areas represent the minimum (*dark*) and maximum (*light*) spread of the lesion across different anterior-posterior levels of BLA (-2.12, -2.56, and -2.80 from bregma), condensed in one level for illustration. BLA, basolateral nucleus of the amygdala; CeA, central nucleus of the amygdala, op., optical tract. **(b)** ET-1 lesion reduced freezing during fear conditioning ($F_{(2,31)} = 3.98$, $p = 0.02$, day 21) at both ET-1/Control (blue, $p = 0.021$, $n = 10$) and ET-1/NeuroD1 (magenta, $p = 0.019$, $n = 14$) groups, compared to Saline/Saline group (black, $n = 10$). Reduced freezing ($F_{(2,31)} = 3.45$, $p = 0.044$) was also observed on the next day (day 22) in both ET-1/Control ($p= 0.030$) and ET-1/NeuroD1 ($p = 0.031$) groups. Rats were then infused with control virus or NeuroD1 and re-tested 3 weeks later ($F_{(2,31)} = 5.86$, $p = 0.006$, day 45). In the ET-1/NeuroD1 group, freezing returned to the levels of the Saline/Saline group ($p= 0.81$),

428 and was significantly higher than ET-1/Control group ($p = 0.004$). “x” denotes baseline
429 pre-tone freezing levels. Hab, habituation; Cond, conditioning; pre-CS, pre-conditioned
430 stimulus. One-way ANOVA followed by Duncan’s post-hoc test. Data are expressed as
431 mean ± s.e.m. in blocks of two trials. * $P < 0.05$. **(c)** After fear conditioning test,
432 immunostaining of rat brain sections confirmed the injection of NeuroD1-GFP viruses
433 into the BLA (green, left panel), and the NeuroD1-infected cells were mostly NeuN-
434 positive neurons (right panels). Scale bar: 1000 μm.

435

436 **DISCUSSION**

437

438 In this study, we demonstrate that NeuroD1-mediated *in vivo* astrocyte-to-neuron
439 conversion can efficiently regenerate a large number of functional neurons in an
440 ischemic injury model and achieve functional rescue of both motor and cognitive deficits
441 in rodents. The high conversion efficiency is due to the master reprogramming effect of
442 NeuroD1, while the effective neuroregeneration is the result of a combination of the
443 AAV vector and the Cre-FLEX system. One interesting discovery is the persistence of
444 astrocytes at the injury sites after NeuroD1-mediated AtN conversion, indicating that
445 astrocytes would not be depleted after conversion. Another important finding is that
446 besides neuroregeneration from the cell conversion, many injured neurons are
447 preserved after AtN conversion, suggesting a neuroprotective effect when changing
448 reactive astrocytes into functional new neurons. With neuroregeneration and
449 neuroprotection together, we could rescue 70-80% of the lost neurons after ischemic
450 injury and reconstitute the motor cortex with layered structures. This proof-of-principle
451 study demonstrates that a highly efficient neuroregeneration is achievable in adult
452 mammalian brains, opening a new avenue for brain repair using internal glial cells as a
453 source after injury or disease.

454

455 **High efficiency of neuroregeneration through *in situ* cell conversion**

456 Most importantly, our NeuroD1-mediated glia-to-neuron conversion can regenerate a
457 large number of new neurons in the stroke areas, averagely 400 NeuN+ cells/mm^2,
458 which is about 100 times of the internal neurogenesis capability in the adult mouse
459 cortex or striatum after ischemic stroke [2-5]. Such remarkable neuroregeneration efficacy
460 is also unmatchable by the typically low efficiency of neuroregeneration after stem cell
461 engraftment. We believe that efficient neuroregeneration is critical for functional repair,
462 because small numbers of new neurons either fail to survive in an injury environment or
463 are insufficient to rebuild neural circuits. This may partly explain why modulating
464 endogenous adult neurogenesis through various approaches so far has not yet resulted
465 in an effective therapy for stroke, possibly due to limited neural stem cell niches in the
466 adult brain [1, 34]. In contrast to modulating endogenous neural stem cells, our *in situ* cell

467 conversion approach makes use of reactive glial cells that are closely associated with
468 neural injury throughout the nervous system for *in situ* regeneration and repair.

469 As one of the efficient vehicles for gene delivery, AAV has been extensively used
470 in the central nervous system for many purposes, such as gene expression and circuit
471 mapping [35]. It has also been used as therapeutic vectors for treatments of neurological
472 disorders. AAV has advantages of high infection rate and long-lasting expression with
473 low pathogenicity. For *in situ* AtN conversion, compared to the retroviruses used in the
474 previous study[13], AAV also has the advantage of infecting both dividing and non-dividing
475 astrocytes, leaving the AtN conversion unrestrained by the number of dividing
476 astrocytes at the viral injection. On the other hand, because AAV can infect both
477 dividing and non-dividing cells, it becomes critical to target glial cells specifically with
478 glia-specific promoters. However, the use of glia-specific promoters also generates a
479 dilemma in which the glial promoter itself become silenced or at least inhibited by the
480 neural transcription factor expressed under the control of the glial promoter. Silencing
481 glial promoter by the neural transcription factor during glia-to-neuron conversion
482 process imposes a negative feedback on the expression level of the neural transcription
483 factor, leading to low conversion efficiency. To overcome this negative feedback effect,
484 we developed a Cre-FLEX system that separates the GFAP promoter from NeuroD1
485 expression so that NeuroD1 expression will not be inhibited during AtN conversion. This
486 is achieved by targeting astrocytes with astrocyte-specific GFAP::Cre AAV vector but
487 expressing NeuroD1 in a different AAV vector under the control of CAG promoter. After
488 Cre-mediated recombination, NeuroD1 will be highly expressed in astrocytes under a
489 more universal CAG promoter to convert astrocytes efficiently into neurons. With this
490 engineered Cre-FLEX AAV system, we demonstrate here that ectopic expression of
491 NeuroD1 in reactive astrocytes following ischemic injury of mouse motor cortex can
492 regenerate >40% of lost neurons, an unprecedented neuroregeneration efficiency
493 compared to classical pharmacological or genetic interventions, which typically
494 regenerate <1% of lost neurons. For example, previous studies have reported the
495 activation of adult neurogenesis after stroke[5, 36], but the number of new neurons
496 generated through modulating internal neurogenesis is ~2-8 $NeuN^+$ neurons/mm^2 [2-5].
497 When considering the actual neuronal density in the brain, which is ~1000 neurons/mm^2

498 [37], it may not be too difficult to understand why so many clinical trials on stroke have
499 failed over the past 30 years [38]. In contrast, our *in vivo* AtN conversion technology
500 makes use of local astrocytes that are surrounding every single neuron to regenerate
501 new neurons wherever neural injury occurs, breaking the bottleneck of classical adult
502 neurogenesis that is limited in certain niches. More importantly, by using the AAV Cre-
503 FLEX system to express NeuroD1 in reactive astrocytes, we now achieve
504 neuroregeneration of ~400 $NeuN^+$ neurons/mm^2, bringing brain repair into a new level
505 with a sufficient number of new neurons to reconstruct the damaged brain structures.
506 With such a high neuroregeneration efficiency, plus additional neuroprotective effect, we
507 demonstrate that the ischemic-injured motor cortex can be gradually reconstituted, and
508 the motor function can be significantly improved.
509 The use of Cre recombinase might raise concerns regarding its possible toxicity[39]
510 [40] [41]. However, we designed our AAV system so that Cre is controlled by GFAP
511 promoter, which will be silenced once NeuroD1 is expressed in astrocytes during the
512 early transitional period of astrocyte-to-neuron conversion process. Indeed, this has
513 been confirmed with Cre immunostaining following NeuroD1 infection (Suppl. Figure
514 5a). In control group (GFAP::Cre + FLEX-GFP), the Cre expression level increased in
515 reactive astrocytes from 4 days to 17 days post infection (dpi), as expected (Suppl.
516 Figure 5a, top row). In NeuroD1 group (GFAP::Cre + FLEX-NeuroD1-GFP), however,
517 Cre was only detected in NeuroD1-GFP positive cells at 4 dpi before conversion but
518 disappeared at 17 dpi, indicating the silence of GFAP promoter once NeuroD1 is
519 expressed (Suppl. Figure 5a, bottom row). Note that in NeuroD1 group, the converted
520 neurons (green) all lacked Cre signal (red), and the remaining Cre signal was not in
521 converted cells.
522 Another concern is the continuous expression of NeuroD1 in converted neurons
523 after Cre-mediated recombination. In fact, NeuroD1 is an endogenous neural
524 transcription factor that is not only expressed during early brain development but also in
525 the adult neural stem cells as well [42, 43]. During our immunostaining analysis of NeuroD1
526 after infection, low level of NeuroD1 expression can be detected in the non-infected pre-
527 existing neurons as well (Suppl. Figure 5b-c). To more directly address whether
528 overexpression of NeuroD1 might impair neuronal functions, we performed brain slice

529 recordings in NeuroD1-GFP converted neurons after 13 months of NeuroD1 infection in
530 mouse brains. The NeuroD1-converted neurons not only survived well after one year,
531 but also displayed repetitive action potentials and synaptic responses (Suppl. Figure
532 5d), suggesting that the possible side effect of NeuroD1 is minimal, if any.
533
534 **Structural support for functional rescue**
535 An exciting finding of this study is that *in situ* AtN conversion can functionally rescue the
536 motor and memory deficits caused by ischemic injury in rodent models. This functional
537 rescue is based on structural changes including both cellular conversion and circuit
538 rebuilding after NeuroD1-treatment. Importantly, we have observed a mixture of
539 NeuroD1-converted neurons together with non-converted neurons in the injury areas
540 after NeuroD1-treatment, suggesting that the repaired brain circuitry is an integration of
541 both newly generated and pre-existing neurons. The fact that NeuroD1-treatment can
542 rescue over 70% of neurons in ischemic injured motor cortex provides necessary
543 structural basis for motor functional recovery. Similarly, a reversal of the memory deficit
544 induced by an amygdala lesion suggests a restoration of the neural circuits in the BLA
545 following NeuroD1 treatment.
546
547 **Perspective on therapeutic potential**
548 The molecular and cellular neuroscience research over the past several decades has
549 gained much insight into the brain structure and function as well as the pathological
550 changes after brain injury. However, therapeutic treatments for effective brain repair has
551 significantly lagged behind. In fact, most of the clinical trials on CNS disorders such as
552 stroke and Alzheimer's disease have largely failed over the recent years [38, 44]. One of
553 the most important reasons is that previous clinical trials cannot regenerate sufficient
554 number of functional neurons to replace the lost neurons after injury. Because neurons
555 are the fundamental building blocks of brain circuits, it is pivotal to have sufficient
556 number of functional new neurons in order to rebuild the impaired neural networks after
557 injury or disease. For example, if one million neurons die after brain injury, simply
558 generating 10,000 neurons may not be sufficient to achieve significant functional repair.
559 It might require regenerating 100,000 or 200,000 new neurons to start really meaningful

560 neural repair. In other words, it might need regenerating at least 10% to 50% of the lost
561 neurons in order to reconstruct the brain circuits that are disrupted by neural injury. The
562 precise threshold in terms of the percentage of new neurons regenerated, whether 10%
563 or 50% of the lost neurons, may vary according to the type of injury or the location in the
564 CNS. Nevertheless, without sufficient number of new neurons added to the injured
565 neural circuitry, it will be difficult to fully restore the lost brain functions solely relying
566 upon the internal compensation mechanisms. Similarly, any serious neurodegenerative
567 disorders such as Alzheimer's disease and Parkinson's disease may also require an
568 effective neuroregeneration approach to reverse the disease symptoms [45].
569 Different from previous pharmacological modulation or stem cell transplantation,
570 our *in vivo* AtN conversion approach makes use of the enormous reservoir of internal
571 glial cells in the CNS to regenerate new neurons. Because glial cells are widely
572 distributed throughout the brain and spinal cord, and more importantly, glial cells can
573 divide to regenerate themselves, the resource for internal neural conversion is
574 enormous. In theory, it is possible to regenerate new neurons anywhere and anytime in
575 the brain so long as the reactive glial cells are surviving the injury. However, if a neural
576 injury is so severe that most glial cells have died, then it may require injection of new
577 cell source such as stem cells and immature neurons, or even glial cells, for neural
578 repair.
579 With the successful development of the highly efficient neuroregeneration
580 approach that can regenerate 40% of the lost neurons and protect additional 40% of
581 injured neurons, we predict that our NeuroD1-mediated AtN conversion technology is
582 one step closer toward a possible gene therapy for brain repair. For example, if a
583 patient is diagnosed with a focal stroke or focal brain injury under MRI scanning,
584 NeuroD1 AAV particles can be locally injected into the injury areas to regenerate new
585 neurons and restore neuronal functions. From a broader perspective, such *in situ* cell
586 conversion therapy may be applied for tissue repair not only in CNS[18], but also in a
587 variety of organs such as pancreas, heart, and liver [46-51]. Importantly, local injection of a
588 small amount of AAV particles may be a preferred route over systemic administration of
589 a large amount of AAV particles, given recent success of local AAV injection in the
590 retina[52] but a disastrous outcome of intravenous AAV injection[53].

ACKNOWLEDGEMENT:

This work was supported by grants from National Institutes of Health (AG045656) and Alzheimer's Association (ZEN-15-321972) to G.C. It was also supported by Charles H. Smith Endowment Fund for Brain Repair and Verne M. Willaman Endowment Fund from the Pennsylvania State University to G.C. The rat fear conditioning test was supported by NIMH grant K99-MH-105549 to F.H.D-M.; NIMH grants R37-MH058883 and P-50-MH-086400 to G.J.Q, and a grant from the University of Puerto Rico President's Office to G.J.Q. We would like to thank Matthew Keefe and Joseph Gyekis for careful proof reading of our manuscript. We would also like to thank all the Chen lab members for rigorous discussing throughout this project over the past 5 years.

602 **REFERENCE**:

603

604 1. Ming, G.L. & Song, H. Adult neurogenesis in the mammalian brain: significant answers
605 and significant questions. *Neuron* **70**, 687-702 (2011).
606 2. Tobin, M.K. et al. Neurogenesis and inflammation after ischemic stroke: what is known
607 and where we go from here. *J Cereb Blood Flow Metab* **34**, 1573-1584 (2014).
608 3. Magnusson, J.P. et al. A latent neurogenic program in astrocytes regulated by Notch
609 signaling in the mouse. *Science* **346**, 237-241 (2014).
610 4. Sun, X. et al. New striatal neurons form projections to substantia nigra in adult rat brain
611 after stroke. *Neurobiol Dis* **45**, 601-609 (2012).
612 5. Arvidsson, A., Collin, T., Kirik, D., Kokaia, Z. & Lindvall, O. Neuronal replacement
613 from endogenous precursors in the adult brain after stroke. *Nat Med* **8**, 963-970 (2002).
614 6. Faiz, M. et al. Adult Neural Stem Cells from the Subventricular Zone Give Rise to
615 Reactive Astrocytes in the Cortex after Stroke. *Cell stem cell* **17**, 624-634 (2015).
616 7. Benner, E.J. et al. Protective astrogenesis from the SVZ niche after injury is controlled by
617 Notch modulator Thbs4. *Nature* **497**, 369-373 (2013).
618 8. Lindvall, O. & Kokaia, Z. Stem cells for the treatment of neurological disorders. *Nature*
619 **441**, 1094-1096 (2006).
620 9. Bliss, T., Guzman, R., Daadi, M. & Steinberg, G.K. Cell transplantation therapy for
621 stroke. *Stroke; a journal of cerebral circulation* **38**, 817-826 (2007).
622 10. George, P.M. & Steinberg, G.K. Novel Stroke Therapeutics: Unraveling Stroke
623 Pathophysiology and Its Impact on Clinical Treatments. *Neuron* **87**, 297-309 (2015).
624 11. Jandial, R. & Snyder, E.Y. A safer stem cell: on guard against cancer. *Nat Med* **15**, 999-
625 1001 (2009).
626 12. Goldman, S.A. Stem and Progenitor Cell-Based Therapy of the Central Nervous System:
627 Hopes, Hype, and Wishful Thinking. *Cell Stem Cell* **18**, 174-188 (2016).
628 13. Guo, Z. et al. In vivo direct reprogramming of reactive glial cells into functional neurons
629 after brain injury and in an Alzheimer's disease model. *Cell stem cell* **14**, 188-202 (2014).
630 14. Grande, A. et al. Environmental impact on direct neuronal reprogramming in vivo in the
631 adult brain. *Nat Commun* **4**, 2373 (2013).
632 15. Niu, W. et al. In vivo reprogramming of astrocytes to neuroblasts in the adult brain. *Nat*
633 *Cell Biol* **15**, 1164-1175 (2013).
634 16. Torper, O. et al. Generation of induced neurons via direct conversion in vivo. *P Natl*
635 *Acad Sci USA* **110**, 7038-7043 (2013).
636 17. Su, Z., Niu, W., Liu, M.L., Zou, Y. & Zhang, C.L. In vivo conversion of astrocytes to
637 neurons in the injured adult spinal cord. *Nat Commun* **5**, 3338 (2014).
638 18. Li, H. & Chen, G. In Vivo Reprogramming for CNS Repair: Regenerating Neurons from
639 Endogenous Glial Cells. *Neuron* **91**, 728-738 (2016).
640 19. Liu, Y. et al. Ascl1 Converts Dorsal Midbrain Astrocytes into Functional Neurons In
641 Vivo. *J Neurosci* **35**, 9336-9355 (2015).
642 20. Heinrich, C. et al. Directing astroglia from the cerebral cortex into subtype specific
643 functional neurons. *PLoS biology* **8**, e1000373 (2010).
644 21. Heinrich, C. et al. Sox2-mediated conversion of NG2 glia into induced neurons in the
645 injured adult cerebral cortex. *Stem Cell Reports* **3**, 1000-1014 (2014).

646 22. Brulet, R. et al. NEUROD1 Instructs Neuronal Conversion in Non-Reactive Astrocytes.
647 *Stem Cell Reports* **8**, 1506-1515 (2017).
648 23. Windle, V. et al. An analysis of four different methods of producing focal cerebral
649 ischemia with endothelin-1 in the rat. *Experimental neurology* **201**, 324-334 (2006).
650 24. Roome, R.B. et al. A reproducible Endothelin-1 model of forelimb motor cortex stroke in
651 the mouse. *J Neurosci Methods* **233**, 34-44 (2014).
652 25. Hughes, P.M. et al. Focal lesions in the rat central nervous system induced by endothelin-
653 1. *Journal of neuropathology and experimental neurology* **62**, 1276-1286 (2003).
654 26. Fuxe, K. et al. Endothelin-1 induced lesions of the frontoparietal cortex of the rat. A
655 possible model of focal cortical ischemia. *Neuroreport* **8**, 2623-2629 (1997).
656 27. Ojala, D.S., Amara, D.P. & Schaffer, D.V. Adeno-associated virus vectors and
657 neurological gene therapy. *The Neuroscientist : a review journal bringing neurobiology,*
658 *neurology and psychiatry* **21**, 84-98 (2015).
659 28. Atasoy, D., Aponte, Y., Su, H.H. & Sternson, S.M. A FLEX switch targets
660 Channelrhodopsin-2 to multiple cell types for imaging and long-range circuit mapping. *J*
661 *Neurosci* **28**, 7025-7030 (2008).
662 29. Johansen, J.P., Cain, C.K., Ostroff, L.E. & LeDoux, J.E. Molecular mechanisms of fear
663 learning and memory. *Cell* **147**, 509-524 (2011).
664 30. Rogan, M.T., Staubli, U.V. & LeDoux, J.E. Fear conditioning induces associative long-
665 term potentiation in the amygdala. *Nature* **390**, 604-607 (1997).
666 31. Goosens, K.A. & Maren, S. Contextual and auditory fear conditioning are mediated by
667 the lateral, basal, and central amygdaloid nuclei in rats. *Learning & memory* **8**, 148-155
668 (2001).
669 32. Gale, G.D. et al. Role of the basolateral amygdala in the storage of fear memories across
670 the adult lifetime of rats. *The Journal of neuroscience : the official journal of the Society*
671 *for Neuroscience* **24**, 3810-3815 (2004).
672 33. Abeysinghe, H.C., Bokhari, L., Dusting, G.J. & Roulston, C.L. Brain remodelling
673 following endothelin-1 induced stroke in conscious rats. *PLoS One* **9**, e97007 (2014).
674 34. Obernier, K., Tong, C.K. & Alvarez-Buylla, A. Restricted nature of adult neural stem
675 cells: re-evaluation of their potential for brain repair. *Frontiers in neuroscience* **8**, 162
676 (2014).
677 35. Rajasethupathy, P., Ferenczi, E. & Deisseroth, K. Targeting Neural Circuits. *Cell* **165**,
678 524-534 (2016).
679 36. Parent, J.M., Vexler, Z.S., Gong, C., Derugin, N. & Ferriero, D.M. Rat forebrain
680 neurogenesis and striatal neuron replacement after focal stroke. *Annals of neurology* **52**,
681 802-813 (2002).
682 37. Schuz, A. & Palm, G. Density of neurons and synapses in the cerebral cortex of the
683 mouse. *J Comp Neurol* **286**, 442-455 (1989).
684 38. Turner, R.C., Dodson, S.C., Rosen, C.L. & Huber, J.D. The science of cerebral ischemia
685 and the quest for neuroprotection: navigating past failure to future success. *J Neurosurg*
686 **118**, 1072-1085 (2013).
687 39. Lexow, J., Poggioli, T., Sarathchandra, P., Santini, M.P. & Rosenthal, N. Cardiac fibrosis
688 in mice expressing an inducible myocardial-specific Cre driver. *Dis Model Mech* **6**, 1470-
689 1476 (2013).

690 40. Bersell, K. et al. Moderate and high amounts of tamoxifen in alphaMHC-MerCreMer
691 mice induce a DNA damage response, leading to heart failure and death. *Dis Model Mech*
692 **6**, 1459-1469 (2013).
693 41. Pomplun, D., Florian, S., Schulz, T., Pfeiffer, A.F. & Ristow, M. Alterations of
694 pancreatic beta-cell mass and islet number due to Ins2-controlled expression of Cre
695 recombinase: RIP-Cre revisited; part 2. *Horm Metab Res* **39**, 336-340 (2007).
696 42. Kuwabara, T. et al. Wnt-mediated activation of NeuroD1 and retro-elements during adult
697 neurogenesis. *Nat Neurosci* **12**, 1097-1105 (2009).
698 43. Gao, Z. et al. Neurod1 is essential for the survival and maturation of adult-born neurons.
699 *Nat Neurosci* **12**, 1090-1092 (2009).
700 44. Anderson, R.M., Hadjichrysanthou, C., Evans, S. & Wong, M.M. Why do so many
701 clinical trials of therapies for Alzheimer's disease fail? *Lancet* **390**, 2327-2329 (2017).
702 45. di Cervo, V.P.R., Romanov, R.A. & Nature …, S.-G. Induction of functional dopamine
703 neurons from human astrocytes in vitro and mouse astrocytes in a Parkinson's disease
704 model. *Nature …* (2017).
705 46. Li, W. et al. In vivo reprogramming of pancreatic acinar cells to three islet endocrine
706 subtypes. *eLife* **3**, e01846 (2014).
707 47. Qian, L. et al. In vivo reprogramming of murine cardiac fibroblasts into induced
708 cardiomyocytes. *Nature* **485**, 593-598 (2012).
709 48. Song, G. et al. Direct Reprogramming of Hepatic Myofibroblasts into Hepatocytes In
710 Vivo Attenuates Liver Fibrosis. *Cell Stem Cell* **18**, 797-808 (2016).
711 49. Zhou, Q., Brown, J., Kanarek, A., Rajagopal, J. & Melton, D.A. In vivo reprogramming
712 of adult pancreatic exocrine cells to beta-cells. *Nature* **455**, 627-632 (2008).
713 50. Song, K. et al. Heart repair by reprogramming non-myocytes with cardiac transcription
714 factors. *Nature* **485**, 599-604 (2012).
715 51. Rezvani, M. et al. In Vivo Hepatic Reprogramming of Myofibroblasts with AAV Vectors
716 as a Therapeutic Strategy for Liver Fibrosis. *Cell Stem Cell* **18**, 809-816 (2016).
717 52. Pierce, E.A. & Bennett, J. The Status of RPE65 Gene Therapy Trials: Safety and
718 Efficacy. *Cold Spring Harb Perspect Med* **5**, a017285 (2015).
719 53. Hinderer, C. et al. Severe toxicity in nonhuman primates and piglets following high-dose
720 intravenous administration of an AAV vector expressing human SMN. *Hum Gene Ther*
721 (2018).

722